Light diffusion in a radially *N*-layered cylinder

André Liemert and Alwin Kienle
Institut für Lasertechnologien in der Medizin und Meßtechnik, Helmholtzstrasse 12, D-89081 Ulm, Germany
(Received 7 June 2011; revised manuscript received 12 September 2011; published 12 October 2011)

Analytical solutions of the diffusion equation for a radially N-layered cylinder were derived in the steady-state, frequency, and time domains. Solutions for axially infinite and finite cylinders are presented. The derived formulas were compared to a known solution of the diffusion equation for a layered semi-infinite geometry and to Monte Carlo simulations, showing excellent and good agreement, respectively. The analytical solutions were applied to calculate the light propagation in models of the forearm and the finger, demonstrating the improvement in analysis of hemodynamics measurements compared to the formulas used so far.

DOI: 10.1103/PhysRevE.84.041911 PACS number(s): 87.64.Cc, 05.60.Cd, 42.25.Bs

I. INTRODUCTION

Light propagation in biological media is usually described by the radiative transfer equation and its approximations, especially the diffusion equation [1]. The advantage of applying the diffusion equation is that it is possible to derive analytical formulas for a variety of relevant geometries. In general, analytical solutions are much faster and more accurate than numerical solutions. In terms of homogeneous media there are solutions of the diffusion equation available for infinite and semi-infinite geometries [2–5], the parallelepiped [6], the cylinder [7–9], and the sphere [7,10]. Moreover, layered geometries aroused interest because many different parts of the body exhibit layered structures. Several analytical solutions of the layered diffusion equation have been found, e.g., for the laterally infinite layered geometry [11–15] and for the axially layered cylinder [16,17]. For example, these solutions can be used for the reconstruction of the optical properties of the involved layers [11,18]. We note that mathematical methods for obtaining solutions of the heat conduction equation for radially layered geometries are also presented in the literature [19–22].

In this study we present a derivation of solutions of the diffusion equation for a cylinder having an arbitrary number of layers in a radial direction. Formulas are presented for axially infinite and finite cylinders in the steady-state, frequency, and time domains. Comparisons of the derived solutions are shown with a solution of the diffusion equation for a layered semi-infinite medium using a large cylinder diameter and with results obtained by the Monte Carlo method, a numerical solution of the radiative transfer equation.

In biophotonics the derived formulas are, for example, interesting for application of hemodynamics measurement on the extremities, like the leg, the arm, or the finger. These parts of the body can be considered approximately as cylinders, and their anatomy in the radial direction can be considered as layers. In the literature these measurements have been described by simpler models, such as semi-infinite media or layered semi-infinite media [23–26]. The improvement due to the derived formulas is demonstrated for the cases of the forearm and of the finger.

II. THEORY

In this section the Green's function of the diffusion equation is derived for a radially N-layered cylinder geometry using the extrapolated boundary condition (EBC) [4]. Figure 1 shows a scheme of a radially layered cylinder through the plane $z = 0$.

In the following derivation it is assumed that the beam incident perpendicular to the cylinder surface at $z' = 0$ and $\phi' = 0$ is represented by an isotropic point source, which is located in layer 1 at position $\mathbf{r}' = (\rho_1 - 1/\mu'_{t1}, \varphi' = 0, z' = 0)$ using cylindrical coordinates, where $\mu'_t = \mu_a + (1-g)\mu_s$ is the reduced total attenuation coefficient, μ_a is the absorption coefficient, μ_s is the scattering coefficient, and g denotes the anisotropic factor. The steady-state diffusion equation for the Green's function $G(\mathbf{r},\mathbf{r}')$ is given by

$$D\nabla^2 G(\mathbf{r},\mathbf{r}') - \mu_a G(\mathbf{r},\mathbf{r}') = -\delta(\mathbf{r}-\mathbf{r}'), \tag{1}$$

where $D = 1/(3\mu'_t)$ is the diffusion coefficient. By using the integral identity

$$\delta(z-z') = \frac{1}{\pi}\int_0^\infty \cos[k(z-z')]dk, \tag{2}$$

and the Fourier series

$$\delta(\varphi-\varphi') = \frac{1}{2\pi}\sum_{m=-\infty}^{\infty} e^{jm(\varphi-\varphi')}, \tag{3}$$

the source term can be written in cylindrical coordinates as

$$\delta(\mathbf{r}-\mathbf{r}') = \frac{\delta(\rho-\rho')}{2\pi^2\rho}\int_0^\infty \cos[k(z-z')]\sum_{m=-\infty}^{\infty} e^{jm\phi}dk, \tag{4}$$

where $\phi = \varphi - \varphi'$ and $j = \sqrt{-1}$. The Green's function can be expanded in the form

$$G(\mathbf{r},\mathbf{r}') = \frac{1}{2\pi^2}\int_0^\infty \cos[k(z-z')]\sum_{m=-\infty}^{\infty} G_m(\rho,\rho',k)e^{jm\phi}dk. \tag{5}$$

By insertion of Eqs. (4) and (5) in Eq. (1) it follows that $G_m(\rho,\rho',k)$ must satisfy the inhomogeneous modified Bessel differential equation,

$$\left(\frac{\partial^2}{\partial\rho^2} + \frac{1}{\rho}\frac{\partial}{\partial\rho} - \gamma^2 - \frac{m^2}{\rho^2}\right)G_m(\rho,\rho',k) = -\frac{\delta(\rho-\rho')}{D\rho}, \tag{6}$$

 ©2011 American Physical Society

where $\gamma^2 = \mu_{\text{eff}}^2 + k^2$ and $\mu_{\text{eff}} = \sqrt{\mu_a/D}$. The solution of Eq. (6) is [27]

$$G_m^{(p)}(\rho,\rho',k) = \frac{1}{D} I_m(\gamma\rho_<) K_m(\gamma\rho_>), \tag{7}$$

where $\rho_< = \min\{\rho,\rho'\}$, $\rho_> = \max\{\rho,\rho'\}$. $I_m(x)$ and $K_m(x)$ are the modified cylindrical Bessel functions of the first and second kinds. By considering the source-free solution of Eq. (6) [28] an appropriate ansatz for the corresponding Green's function is made by

$$G_m(\rho,\rho',k) = \begin{cases} A_1 I_m(\gamma_1\rho) + B_1 K_m(\gamma_1\rho) + 1/D_1 I_m(\gamma_1\rho_<) K_m(\gamma_1\rho_>), & \rho_2 < \rho \leqslant \rho_1, \\ A_n I_m(\gamma_n\rho) + B_n K_m(\gamma_n\rho), & \rho_{n+1} < \rho \leqslant \rho_n\,, \end{cases} \tag{8}$$

where $\gamma_n = \sqrt{\mu_{an}/D_n + k^2}$ $(n = 1,\ldots,N)$. For defining the layered structure the radial dependent Green's function must satisfy the following boundary conditions:

$$\begin{gathered} G_m(\rho_{1b},\rho',k)=0, \quad n_{n+1}^2 G_m(\rho_n^-,\rho',k)=n_n^2 G_m(\rho_n^+,\rho',k), \\ D_n \partial_\rho G_m(\rho_n^-,\rho',k)=D_{n+1}\partial_\rho G_m(\rho_n^+,\rho',k), \\ G_m(0,\rho',k) < \infty, \end{gathered} \tag{9}$$

where the first equation states the extrapolated boundary condition and $\rho_{1b} = \rho_1 + \rho_b$ denotes the extrapolated radius. The value of ρ_b is given by [5]

$$\rho_b = 2D_1 \frac{1 + R_{\text{eff}}}{1 - R_{\text{eff}}}, \tag{10}$$

where R_{eff} is the angle-averaged probability for reflection at the border to the surrounding medium [4].

After an explicit derivation of the Green's function for a two-, three-, and four-layered cylinder geometry the following solution for the N-layered cylinder can be identified for the outermost layer. Using the start values

$$\begin{aligned} \alpha_{N-1} &= D_{N-1} n_{N-1}^2 K_m'(\gamma_{N-1}\rho_N) I_m(\gamma_N\rho_N) \\ &\quad - D_N n_N^2 K_m(\gamma_{N-1}\rho_N) I_m'(\gamma_N\rho_N), \\ \beta_{N-1} &= D_{N-1} n_{N-1}^2 I_m'(\gamma_{N-1}\rho_N) I_m(\gamma_N\rho_N) \\ &\quad - D_N n_N^2 I_m(\gamma_{N-1}\rho_N) I_m'(\gamma_N\rho_N) \end{aligned} \tag{11}$$

and the downward recursion relations

$$\begin{aligned} \alpha_n &= D_n n_n^2 [I_m(\gamma_{n+1}\rho_{n+1})\alpha_{n+1} \\ &\quad - K_m(\gamma_{n+1}\rho_{n+1})\beta_{n+1}] K_m'(\gamma_n\rho_{n+1}) \\ &\quad - D_{n+1} n_{n+1}^2 [I_m'(\gamma_{n+1}\rho_{n+1})\alpha_{n+1} - K_m'(\gamma_{n+1}\rho_{n+1})\beta_{n+1}] \\ &\quad \times K_m(\gamma_n\rho_{n+1}), \\ \beta_n &= D_n n_n^2 [I_m(\gamma_{n+1}\rho_{n+1})\alpha_{n+1} \\ &\quad - K_m(\gamma_{n+1}\rho_{n+1})\beta_{n+1}] I_m'(\gamma_n\rho_{n+1}) \\ &\quad - D_{n+1} n_{n+1}^2 [I_m'(\gamma_{n+1}\rho_{n+1})\alpha_{n+1} - K_m'(\gamma_{n+1}\rho_{n+1})\beta_{n+1}] \\ &\quad \times I_m(\gamma_n\rho_{n+1}) \end{aligned} \tag{12}$$

until the quantities α_1 and β_1 are obtained leads to the required constants

$$\begin{aligned} A_1 &= \frac{K_m(\gamma_1\rho_1)}{D_1} \frac{K_m(\gamma_1\rho')\beta_1 - I_m(\gamma_1\rho')\alpha_1}{I_m(\gamma_1\rho_1)\alpha_1 - K_m(\gamma_1\rho_1)\beta_1}, \\ B_1 &= \frac{\beta_1}{D_1} \frac{I_m(\gamma_1\rho')K_m(\gamma_1\rho_1) - K_m(\gamma_1\rho')I_m(\gamma_1\rho_1)}{I_m(\gamma_1\rho_1)\alpha_1 - K_m(\gamma_1\rho_1)\beta_1}. \end{aligned} \tag{13}$$

Note that the prime for I_m and K_m describes the derivative [28], e.g.,

$$\begin{aligned} I_m'(\gamma_n\rho_n) &= \gamma_n I_{m+1}(\gamma_n\rho_n) + \frac{m}{\rho_n} I_m(\gamma_n\rho_n), \\ K_m'(\gamma_n\rho_n) &= -\gamma_n K_{m+1}(\gamma_n\rho_n) + \frac{m}{\rho_n} K_m(\gamma_n\rho_n). \end{aligned} \tag{14}$$

Therefore, the homogeneous solution is obtained as

$$\begin{aligned} G^{(h)}(\mathbf{r},\mathbf{r}') = \frac{1}{2\pi^2} \int_0^\infty \cos[k(z-z')] \sum_{m=-\infty}^{\infty} [A_1 I_m(\gamma_1\rho) \\ + B_1 K_m(\gamma_1\rho)] e^{jm\phi} dk. \end{aligned} \tag{15}$$

Note that $e^{jm\phi}$ can be replaced by $\cos(m\phi)$ because the imaginary part cancels out due to the summation over m.

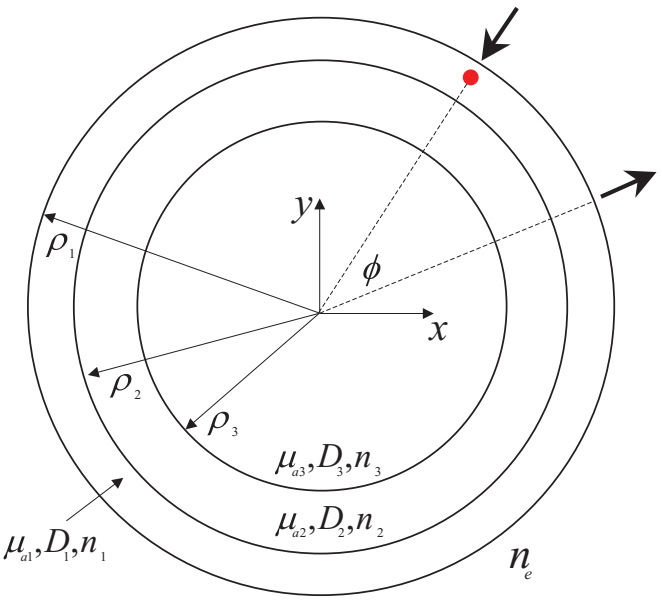

FIG. 1. (Color online) Cross section at $z = 0$ of the radially layered cylinder model. As an example three layers ($N = 3$) are shown.

Thus the Green's function for the outermost cylindrical layer $\rho_2 < \rho \leqslant \rho_1$ becomes

$$G(\mathbf{r},\mathbf{r}') = \frac{e^{-\kappa_1|\mathbf{r}-\mathbf{r}'|}}{4\pi D_1|\mathbf{r}-\mathbf{r}'|} + G^{(h)}(\mathbf{r},\mathbf{r}'), \tag{16}$$

where $|\mathbf{r}-\mathbf{r}'| = \sqrt{\rho^2+\rho'^2-2\rho\rho'\cos(\varphi-\varphi')+(z-z')^2}$ and $\kappa_1 = \sqrt{\mu_{a1}/D_1}$. Note that the first term of Eq. (16) is obtained from the summation of $G_m^{(p)}(\rho,\rho',k)$ over k and m, which leads to the infinite space Green's function caused by an isotropic source.

The Green's function of the time-dependent diffusion equation,

$$\left(\frac{1}{c}\frac{\partial}{\partial t} + \mu_a - D\nabla^2\right)G(\mathbf{r},t,\mathbf{r}',t') = \delta(\mathbf{r}-\mathbf{r}')\delta(t-t'), \tag{17}$$

can be obtained by replacing all real-valued absorption coefficients μ_{an} by complex absorption coefficients $\mu_{an} + j\omega/c_n$, where c_n is the speed of light in layer n (we note that this corresponds to the solution in the frequency domain) and by performing the inverse Fourier transform,

$$G(\mathbf{r},t,\mathbf{r}',t') = \frac{1}{2\pi}\int_{-\infty}^{\infty} G(\mathbf{r},\mathbf{r}',\omega)e^{j\omega(t-t')}d\omega. \tag{18}$$

In this case Eq. (16) becomes

$$G(\mathbf{r},t,\mathbf{r}',t') = \frac{c_1}{[4\pi D_1 c_1(t-t')]^{3/2}}e^{-\mu_{a1}c_1(t-t')}e^{-\frac{|\mathbf{r}-\mathbf{r}'|^2}{4D_1c_1(t-t')}} + \frac{1}{2\pi}\int_{-\infty}^{\infty} G^{(h)}(\mathbf{r},\mathbf{r}',\omega)e^{j\omega(t-t')}d\omega. \tag{19}$$

The remitted light from the cylinder barrel is calculated via Fick's law [29] as

$$R(\varphi,\varphi',z,z') = -D_1\frac{\partial G(\mathbf{r},\mathbf{r}')}{\partial\rho}\,|_{\rho=\rho_1}. \tag{20}$$

In this study we used Fick's law for calculating the reflectance from the cylinder barrel. We note that, especially when the reflectance is considered for a refractive index mismatch between the outermost scattering layer and the surrounding nonscattering medium, the use of a combination of Fick's law and the fluence at the cylinder barrel delivers better agreement compared to Monte Carlo simulations using a Henyey-Greenstein phase function [5].

In the next section the derived formulas are compared to Monte Carlo simulations. Our standard Monte Carlo code was extended for calculation of the light propagation in a turbid cylinder consisting of an arbitrary number of layers, which have arbitrary thicknesses and optical properties. For the phase function a Henyey-Greenstein function was applied using an anisotropy factor of $g = 0.8$.

III. RESULTS

A. Validation

In this section the derived solutions of the diffusion equation are compared first with a solution of the diffusion equation for a different geometry and second with Monte Carlo simulations.

In order to check the correctness of the obtained recursively defined expressions the derived solutions were compared with solutions of the diffusion equation for an N-layered laterally infinite geometry [14]. To this end the radius of the whole cylinder used in the derived formulas was assumed to be sufficiently large ($\rho_1 = 120$ mm), so that the cylinder degenerates approximately to a laterally infinite model. Figure 2 shows the spatially resolved reflectance from a turbid medium having eight layers for the cylindrical model versus the axial direction at $\phi = 0$ (solid curve) and for the laterally infinitely large model (symbols).

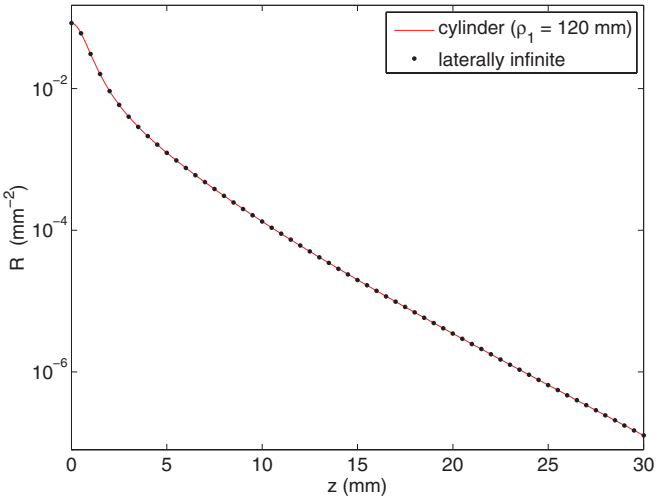

FIG. 2. (Color online) Reflectance vs distance along the z direction for a radially eight-layered cylinder with $\rho_1 = 120$ mm calculated with the derived solutions of the diffusion equation is compared to the corresponding solution of an eight-layered semi-infinitely extended medium.

The optical and geometrical properties are given in Table I using the values listed in column ρ_I for the radii. The refractive index of the surrounding medium is $n_e = 1$. The thicknesses of the layers equal the differences between the corresponding cylinder radii, i.e., $l_i = \rho_i - \rho_{i+1}$. Both curves show an excellent agreement. The relative differences are in the range of 10^{-5}, which are due to the fact that, although $\rho_1 \gg 1/\mu_t'$, the curved cylinder barrel has still a small influence on the reflectance especially at large distances.

Figure 3 shows the spatially resolved reflectance from the radially eight-layered turbid medium whose optical and geometrical properties are given in Table I using the radii given in column ρ_{II} with the exception that now the refractive indices

TABLE I. Optical and geometrical properties of the eight-layered cylinder model.

Layer	μ_s' (mm^{-1})	μ_a (mm^{-1})	ρ_I (mm)	ρ_{II} (mm)	n
1	1.0	0.01	120	10	1.4
2	0.8	0.02	118	8	1.3
3	1.1	0.009	117	7	1.5
4	0.7	0.015	116	6	1.2
5	1.2	0.03	115	5	1.1
6	0.9	0.025	114	4	1.7
7	1.2	0.03	113	3	0.9
8	0.9	0.025	112	2	1.6

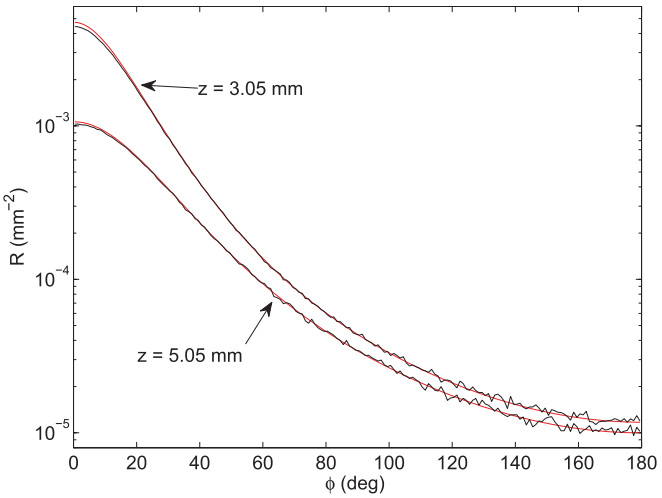

FIG. 3. (Color online) Reflectance vs ϕ obtained from the Monte Carlo simulations (black curves) and from the solution of the diffusion approximation [red (gray) curves].

of the turbid layers and the surrounding medium are 1.4. The reflectance is given versus the angle ϕ and was calculated using the derived analytical solution [red (gray) curves] and the Monte Carlo method (black curves). As indicated in Fig. 3 curves for two different z values are shown.

The reflectance obtained from the solution of the diffusion equation agrees well with that calculated with the Monte Carlo method. Expected differences are seen at small distances where the diffusion approximation breaks down and at large distances due to the noise in the Monte Carlos simulations.

B. Application

This section describes two applications of the derived solutions. The spatially resolved reflectances from a three-layered forearm model and from a four-layered finger model are presented. In all layers a refractive index of 1.4, which is typical for biological media, was assumed. For the surrounding nonscattering medium the same refractive index was chosen because most measurements in the literature were performed with source and detector fibers that were embedded in absorbing media with $n_e \approx 1.4$.

TABLE II. Optical and geometrical properties of the forearm model.

Layer	μ_s' (mm^{-1})	μ_a (mm^{-1})	ρ (mm)
Skin	1.5	0.01	40
Fat	1.0	0.003	39
Muscle	0.5	0.02	35

Figure 4 shows the spatially resolved reflectance along the axial z direction at $\phi = 0$ on the cylinder barrel for the forearm model calculated with the derived analytical solution (solid curve) and the Monte Carlo simulation (circles). The assumed properties for the forearm model are given in Table II. A forearm radius of 40 mm and thicknesses of the skin and the fat layers of 1 and 4 mm, respectively, were used. Both curves show a good agreement except at very small distances. Figure 4 shows also the spatially resolved reflectance for a laterally infinitely extended medium (dashed curve) using the same optical properties and thicknesses for the three layers. Small but significant differences (about 10% at large distances) can be seen in Fig. 4. Thus, even in axial direction the curvature of the forearm has some influence on the noninvasive determination of the hemodynamics in the forearm.

Next, the spatially resolved reflectance versus the ϕ direction at $z = 0$ is compared for the forearm model. Figure 5 shows the reflectance for the same optical and geometrical properties as were applied in Fig. 4. Again, the solution of the radially layered cylinder (solid curve) and the Monte Carlo (symbols) simulations agree well. In contrast, the assumption of a semi-infinite medium with laterally infinitely extended layers (dashed curve) results in large differences compared to the curved geometry. Thus, this solution cannot be applied for spatial reflectance versus the ϕ direction, especially when larger distances are involved.

In the second model we consider measurements of the finger. We assumed that the finger can be approximated by an infinitely long cylinder having four concentric tissue layers.

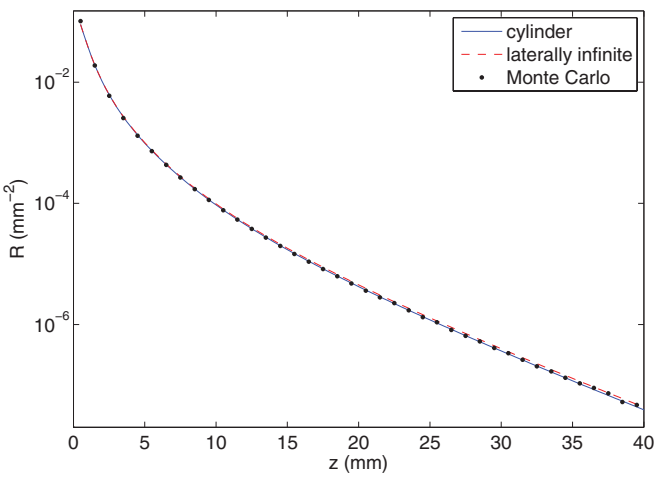

FIG. 4. (Color online) Reflectance vs distance along the z direction for the forearm model.

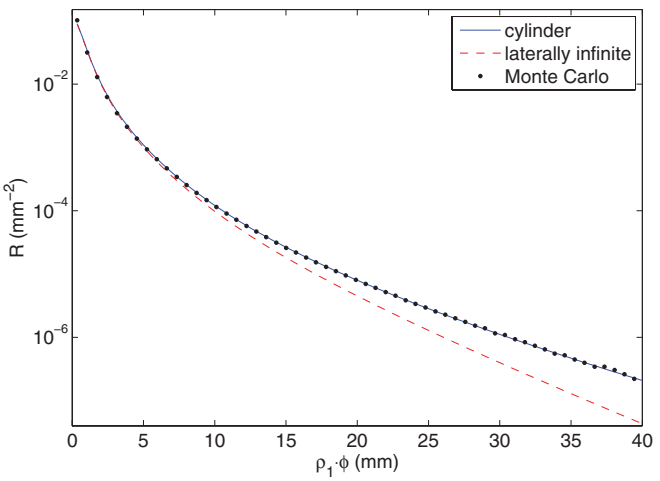

FIG. 5. (Color online) Spatially resolved reflectance along the ϕ direction for the forearm model.

TABLE III. Optical and geometrical properties of the finger model.

Layer	μ_s' (mm^{-1})	μ_a (mm^{-1})	ρ (mm)
Skin	1.5	0.01	8
Fat	1.0	0.003	7
Muscle	0.5	0.02	6
Bone	1.3	0.01	4

The skin, the fat, and the muscle have thicknesses of 1, 1, and 2 mm, respectively, whereas the radius of the bone cylinder is 4 mm. The applied optical and geometrical properties are given in Table III.

Figure 6 compares the spatially resolved reflectance in axial direction for the finger model obtained by the solution of the radially four-layered diffusion equation (dashed curve) and the Monte Carlo method (symbols), delivering again good agreement. The reflectance for the laterally extended medium is also shown (dashed curve). Here, even for the reflectance in axial direction, the differences between the two geometries is large due to the smaller diameter of the whole cylinder.

Finally, in Fig. 7 the resulting reflectance along the ϕ direction for the finger model is compared to the Monte Carlo method and the laterally infinite model. The reflectance derived by solving the diffusion equation for the radially four-layered cylinder (solid curve) is again close to that derived by the Monte Carlo method (symbols). However, differences can be seen at intermediate distances ($\rho_1\phi \approx 5$ mm), whereas at large distances [e.g., at the opposite side of the cylinder relative to the incident beam ($\rho_1\phi \approx 25$ mm)] both curves are close to each other. Contrarily, the reflectance obtained with the laterally infinite model (dashed curve) shows large differences compared to the cylindrical geometry due to the small cylinder radius.

IV. CONCLUSION

Solutions of the diffusion equation for a turbid cylinder having an arbitrary number of layers in the radial direction were derived in the steady-state, frequency, and time domains. The solution for an eight-layered cylinder having a large total diameter was compared to the corresponding solution of the semi-infinite turbid medium, showing excellent agreement. As a further validation the reflectance from an eight-layered turbid cylinder obtained by the derived formulas was compared to a Monte Carlo simulation, resulting in the expected good agreement.

The derived solutions were used to study the light propagation in models of the forearm and the finger assuming three and four layers, respectively. It was shown that for both models the curvature of the extremities has to be considered for measurements in the azimuthal direction and, in the case of the finger model, also in the axial direction. For example, in the case of the finger model the layered semi-infinite geometry, which has been used in the literature so far, has errors up to more than an order of magnitude compared to the derived solutions that consider the actual geometry; see Fig. 7. The differences between the solutions of the radially layered cylinder and the layered semi-infinite medium in the axial direction are smaller for the forearm model but are still significant. Again, the comparison with the Monte Carlo method showed good agreement. Thus, it is possible to apply the solutions of the diffusion equation even for the measurement on the finger, which can be used, e.g., for investigations of pulse oximetry.

The derived analytical formulas deliver solutions of the light propagation in scattering media, which are much faster compared to numerical solutions like the Monte Carlo method, offering the possibility of quickly solving the inverse problem. Furthermore, the analytical solutions are much more exact than numerical methods, which are usually applied to solve the diffusion equation for advanced geometries.

Finally, we note that the derived equations can be used to obtain corresponding solutions of the heat conduction equation [19], as the diffusion equation includes the heat conduction equation as a special case.

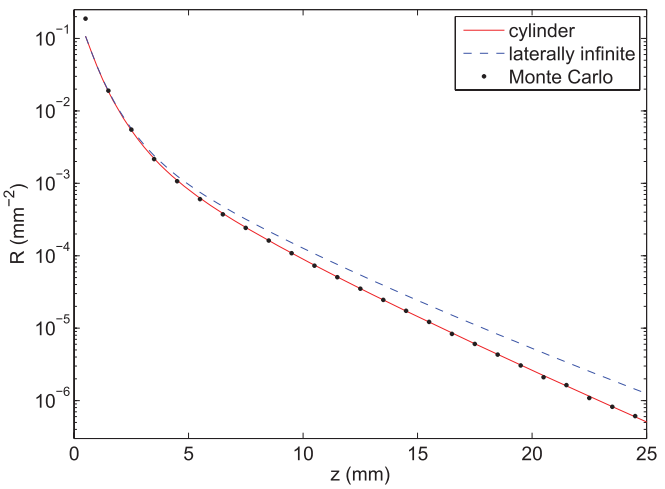

FIG. 6. (Color online) Reflectance vs distance along the z direction for the finger model.

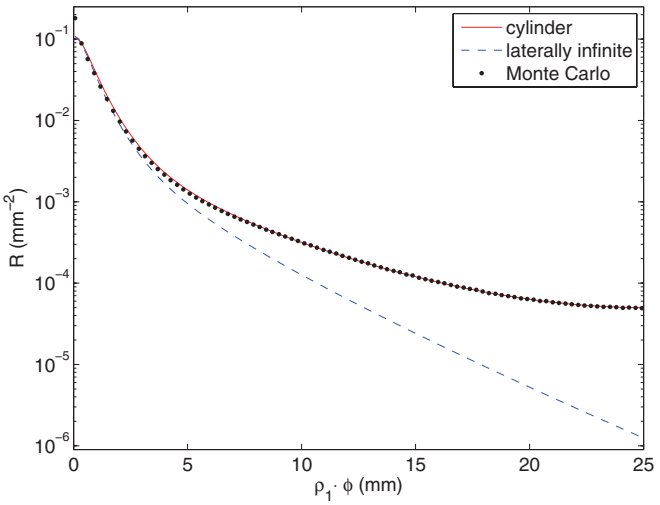

FIG. 7. (Color online) Spatially resolved reflectance along the ϕ direction for the finger model.

ACKNOWLEDGMENT

We acknowledge the support by the European Union (nEUROPt, Grant agreement No. 201076).

APPENDIX

This Appendix presents the Green's function of the diffusion equation for the more general case of a radially N-layered cylinder with a finite length L in the axial direction using the zero-boundary conditions at $z = 0$ and $z = L$. In this case the integral identity equation (2) is replaced by the completeness relation

$$\delta(z - z') = \frac{2}{L}\sum_{k=1}^{\infty}\sin(\lambda_k z)\sin(\lambda_k z'), \quad \lambda_k = k\pi/L. \tag{A1}$$

Thus, the solution of the inhomogeneous Bessel differential equation for the outermost cylindrical layer $\rho_2 < \rho \leqslant \rho_1$ becomes

$$G_{km}(\rho,\rho') = \frac{1}{D_1} I_m(\gamma_1\rho_<)K_m(\gamma_1\rho_>) + A_1 I_m(\gamma_1\rho) + B_1 K_m(\gamma_1\rho), \tag{A2}$$

where $\gamma_n = \sqrt{\mu_{an}/D_n + \lambda_k^2}$ $(n = 1,\ldots,N)$. The Green's function for a finite cylinder model is given by

$$G(\mathbf{r},\mathbf{r}') = \frac{1}{\pi L}\sum_{k=1}^{\infty}\sin(\lambda_k z)\sin(\lambda_k z')\sum_{m=-\infty}^{\infty}\cos(m\phi)G_{km}(\rho,\rho'), \tag{A3}$$

where $0 \leqslant z \leqslant L$. This representation can also be separated in the corresponding particular and homogeneous part,

$$G(\mathbf{r},\mathbf{r}') = \frac{1}{\pi D_1 L}\sum_{k=1}^{\infty}\sin(\lambda_k z)\sin(\lambda_k z')K_0(\gamma_1|\rho - \rho'|) + G^{(h)}(\mathbf{r},\mathbf{r}'), \tag{A4}$$

where

$$G^{(h)}(\mathbf{r},\mathbf{r}') = \frac{1}{\pi L}\sum_{k=1}^{\infty}\sin(\lambda_k z)\sin(\lambda_k z')\sum_{m=-\infty}^{\infty}[A_1 I_m(\gamma_1\rho) + B_1 K_m(\gamma_1\rho)]\cos(m\phi). \tag{A5}$$

Here the particular part becomes the Green's function for a laterally infinite slab of thickness L with the optical properties of the outermost cylindrical layer.

[1] A. Ishimaru, *Wave Propagation and Scattering in Random Media* (Academic, New York, 1978).

[2] M. S. Patterson, B. Chance, and B. C. Wilson, Appl. Opt. **28**, 2331 (1989).

[3] T. J. Farrell, M. S. Patterson, and B. C. Wilson, Med. Phys. **19**, 879 (1992).

[4] R. C. Haskell, L. O. Svaasand, T. T. Tsay, T. C. Feng, M. S. McAdams, and B. J. Tromberg, J. Opt. Soc. Am. A **11**, 2727 (1994).

[5] A. Kienle and M. S. Patterson, J. Opt. Soc. Am. A **14**, 246 (1997).

[6] A. Kienle, J. Opt. Soc. Am. A **22**, 1883 (2005).

[7] S. R. Arridge, M. Cope, and D. T. Delpy, Phys. Med. Biol. **37**, 1531 (1992).

[8] A. Zhang, D. Piao, C. F. Bunting, and B. W. Pogue, J. Opt. Soc. Am. A **27**, 648 (2010).

[9] A. Liemert and A. Kienle, Opt. Express **18**, 9456 (2010).

[10] A. Sassaroli, F. Martelli, G. Zaccanti, and Y. Yamada, Appl. Opt. **40**, 185 (2001).

[11] A. Kienle, M. S. Patterson, N. Dögnitz, R. Bays, G. Wagnières, and H. van den Bergh, Appl. Opt. **37**, 779 (1998).

[12] J. M. Tualle, H. L. Nghiem, D. Ettori, R. Sablong, E. Tinet, and S. Avrillier, J. Opt. Soc. Am. A **21**, 24 (2004).

[13] X. C. Wang and S. M. Wang, Waves Random Complex Media **16**, 121 (2006).

[14] A. Liemert and A. Kienle, J. Biomed. Opt. **15**, 025003 (2010).

[15] A. Liemert and A. Kienle, J. Biomed. Opt. **15**, 025002 (2010).

[16] F. Martelli, S. Sassaroli, S. Del Bianco, and G. Zaccanti, Phys. Med. Biol. **52**, 2827 (2007).

[17] A. Liemert and A. Kienle, Opt. Express **18**, 9266 (2010).

[18] F. Martelli, M. Bassani, L. Alianelli, L. Zangheri, and G. Zaccanti, Phys. Med. Biol. **45**, 1359 (2000).

[19] A. Mandelis, *Diffusion-Wave Fields: Mathematical Methods and Green Functions* (Springer, New York, 2001).

[20] C. Wang, A. Mandelis, and Y. Liu, J. Appl. Phys. **97**, 014911 (2005).

[21] C. Wang, Y. Liu, A. Mandelis, and J. Shen, J. Appl. Phys. **101**, 083503 (2007).

[22] G. Xie, J. Zhang, L. Liu, C. Wang, and A. Mandelis, J. Appl. Phys. **109**, 113534 (2011).

[23] M. Ferrari, T. Binzoni, and V. Quaresima, Philos. Trans. R. Soc. London, Ser. B **352**, 677 (1997).

[24] D. T. Delpi and M. Cope, Philos. Trans. R. Soc. London, Ser. B **352**, 649 (1997).

[25] D. Geraskin, P. Platen, J. Franke, and M. Kohl-Bareis, Proc. SPIE **6629**, 66290P (2007).

[26] T. Hamaoka, K. K. McCully, V. Quaresima, K. Yamamoto, and B. Chance, J. Biomed. Opt. **12**, 062105 (2007).

[27] V. A. Markel and J. C. Schotland, Phys. Rev. E **70**, 056616 (2004).

[28] M. Abramowitz and I. A. Stegun, *Handbook of Mathematical Functions with Formulas, Graphs, and Mathematical Tables* (Dover, New York, 1964).

[29] F. Martelli, S. Del Bianco, A. Ismaelli, and G. Zaccanti, *Light Propagation through Biological Tissue* (SPIE Press, Bellingham, WA, 2010).